This article has been published in: RSC Adv. (2016) 6, 45265–45278. doi:10.1039/C6RA02373H

Title: Submicron-to-nanoscale structure characterization and organization of crystals in dentin bioapatites.

Authors: Manuel Toledano[1*], Fátima S. Aguilera[1], Estrella Osorio[1], Modesto T. López-López[2], Inmaculada Cabello[1], Manuel Toledano-Osorio[1], Raquel Osorio[1].

Institution: [1]University of Granada, Faculty of Dentistry, Dental Materials Section.
[2]University of Granada, Faculty of Science, Applied Physics Department.

Address: [1]University of Granada, Faculty of Dentistry, Dental Materials Section
Colegio Máximo de Cartuja s/n
18071 – Granada - Spain.
[2]University of Granada, Faculty of Science, Applied Physics Department
Fuente Nueva s/n
18071 – Granada – Spain.

*Corresponding author: Prof. Manuel Toledano
University of Granada, Faculty of Dentistry
Dental Materials Section
Colegio Máximo de Cartuja s/n
18071 – Granada - Spain.
Tel.: +34-958243788
Fax: +34-958240809
Email: toledano@ugr.es

Abstract

The aim of this research was to ascertain the crystal morphology, and to assess the ultrastructure and texture changes of sound (SD) and caries-affected dentin (CAD) after being restored with Zn-free and Zn-containing amalgam. Dentin surfaces were studied by X-ray diffraction (μXRD^2), and Transmission Electron Microscopy (TEM) through selected area diffraction (SAED) and bright-field (BF) imaging. Crystals, at the dentin surface, were identified as hydroxyl-apatite with augmented crystallographic maturity, crystallite and grain sizes, and lower microstrain, in CAD dentin after Zn-containing amalgam removal, at 310 plane. This group, at this reflection, achieved lower microstrain than before amalgam placement. Opposed trend was followed at 002 reflection. Texture increased in CAD at both reflections, after the removal of Zn-containing amalgams. Crystallinity increased in SD after amalgam restorations at 002 and 310 reflections. In CAD, crystallinity decreased after amalgam restorations at 002 plane. Block-like and needle-like apatite crystals constituted the bulk of minerals in SD. Needle-like apatite crystals were observed, in CAD surfaces, before and after Zn-free amalgam restorations. Polyhedral and rounded drop-like shaped crystals characterized the CAD surfaces before Zn-containing amalgam placement. After the restoration removal, plate-like polygons and three-dimensional agglomerated crystals were determined. Crystallites, with improved crystallographic orientation, became shorter and thinner in CAD treated with Zn-containing amalgams, thus increasing mineralization and maturity.

1. Introduction

Dentin is a mineralized connective tissue that constitutes the bulk of the tooth. Dentin is a hydrated structure, composed of a continuous network of type I collagen fibrils and mineral. The mineral phase in dentin mainly consists of carbonate-substituted hydroxyapatite (HAp) [Ca10(PO4)6-x(OH)2-y](CO3)x+y, where $0 \leq x \leq 6$, $0 \leq y \leq 2$[1]. Each mineralized fibril is a composite of a collagen framework and very thin needle- and plate-shaped crystals of apatite crystallites (48%). Their c-axes grow and are well aligned with the collagen fibrils, almost always resulting in oriented electron diffraction patterns[2], showing a preferred crystal orientation[1]. The crystals are organized in layers that traverse the fibril axis[2,3]. Dentin contains multiple closely packed dentinal tubules, of about 2 μm in diameter, surrounded by a cuff of highly mineralized peritubular dentin, and intertubular dentin between them[3]. With regards to crystal structures, peritubular dentin is comprised of small, ca. 250 Å, equal side microcrystals whilst the intertubular dentin is characterized by typical larger hexagonal crystalline plates[1]. The interactions between collagen and nano-size mineral crystallites give raise to the stiffness of the dentin structure[3].

The size of the apatite crystals in dentin is roughly 5 x 30 x 100 nm, they have less calcium than stoichiometric HAp and contains 4-5% carbonate. Lower calcium content and higher carbonate content leads to higher acidic solubility of the apatite crystals than stoichiometric apatite and, therefore, higher vulnerability to carious attack[4]. Not only dentin crystallites are extremely small, they are often described as “poorly crystalline” because of the broad X-ray diffraction peaks, which is thought to arise from the incorporation of impurities, such as carbonate, sodium and magnesium ions, and non-stoichiometry of the biogenic minerals[5].

Dentin demonstrates hierarchical structure at the nano- and microscales with organic and inorganic components organized in sub-structures optimized by evolution to withstand environmental stresses associated with their biological function[3]. In the oral environment, teeth are subjected to challenges provided by mechanical stresses from mastication and para-functional habits. Load cycling has been widely used as potential aging method that, additionally, stimulates challenges *in vitro*, *i.e.*, dentin remineralization[6]. Reincorporation of mineral into the demineralized dentin matrix is important since the mineral precipitated may become a constant site for further nucleation, and the remineralized subsurface of the tissue may be more resistant to subsequent acid attack[7], to withstand the progression of the carious process.

Caries demineralized dentin is mainly caused by exposure to acidic conditions with pH less than critical when the mineral tends to dissolve until the solution becomes saturated. Carious dentin is described in terms of two altered layers, an outer or infected layer and an inner or affected layer[8]. Dental amalgam and resin composite are used by dentists to restore teeth diseased by dental caries. Failure of restorations is mainly due to secondary caries in resin composites and to tooth fracture in amalgam restorations. *In vivo* biodegradation of the bond between the composite and tooth is considered a particularly critical contributor to secondary loss of adhesion, microleakage and decay[9-11]. Improved clinical performance of amalgam restorations, as measured by a reduction in marginal fracture, may be related to the presence of zinc in the amalgam alloy[12]. It has been demonstrated, previously, that Zn-containing amalgam restorations submitted to three weeks of load cycling promoted intrafibrillar mineralization of the partially mineral-depleted caries-affected dentin. These minerals were identified as calcium-phosphate deposits, and crystals as HAp with augmented crystallographic maturity but with some components of lattice distortion[13].

X-ray diffraction (XRD) is one of the most powerful techniques to study the hierarchical structure of biological mineral such as teeth and bone. The traditional technique was powder XRD, but is not applicable for small specific areas, it poses a destructive technique, and it is not effective in the identification of small quantities of secondary mineral. Micro-beam techniques were, then, proposed but for samples with relatively large grain size, inhomogeneous phase distribution and preferred orientation. The development of micro-XRD (μ-XRD) instruments has overcome many of these drawbacks and it is now possible to apply this nondestructive technique to study selected areas of specimens down to 50 μm in diameter *in situ*[3]. Thus, analytical and morphological data may be obtained in the same sample, as HAp is going to be assessed peak-to-peak approach using the Scherrer formulae. The line profile analysis uses the broadening of the 002 and 300 reflections, to evaluate the length of the coherent domains along the c-axis and along a direction perpendicular to it. The c-axis of crystallites in dentin, as in other mature hard tissues, is distributed along extended collagen fibers[14]. As it was proposed previously[13], it is recommended in addition, to determine the grain size and lattice strain accordingly determined by measuring the deviation of line profile from perfect crystal diffraction, and so the preferred orientation of crystallites. The crystallites are the region in the specimen diffracting X-rays coherently and independently, whereas the strain is due to different displacement of the atoms with respect to their reference position in a perfect lattice. Size broadening is independent from the order of the reflection, whereas strain broadening is order-dependent[14].

Transmission electron microscopy (TEM) and selected area electron diffraction pattern (SAED) have been employed to characterize the size, shape and structure of nanomaterials. Morphological analyses can be conducted from the μm scale to atomic

scale[15]. The SAED pattern recorded on some specific area exhibits diffraction spots/rings with interplanar spacing that could be indexed according to the mineral nature[16].

The dimensions and morphology of HAp crystals affect its mechanical properties[17] and predetermine its clinical service. It is recommended to understand the influence of the geometry of the ultrastructural elements, such as size and preferred orientation (texture) of dentin nanocrystallites on the overall mechanical properties[3]. Therefore, a systematic investigation of tooth ultrastructures is needed to understand this correlation, as sizes, morphology and structure of nanoparticles determine their reactivity and biomedical properties; e.g, poor HAp is low fracture toughness and low degradation properties, limiting its clinical application in hard tissues[17].

The purpose of the present study was to investigate the crystal morphology, structure and texture of sound and caries-affected dentin after amalgam restorations. The null hypothesis is that there are no differences in crystal morphology, structure and texture between sound and caries-affected dentin after removal of Zn-free *vs.* Zn-containing amalgam restorations.

2. Materials and Methods

2.1. Specimens preparation.

Eight extracted carious third molars without opposing occlusion were employed for the study. They were stored in 0.01% (w/v) thymol at 4º C for less than 1 month. Teeth were collected after written patients' informed consent (20 to 40 yr of age), under a protocol approved by the Institution Review Board (891/2014). Specimens were randomly assigned to two groups (n=4) according to the type of amalgam to be used (with or without zinc). The inclusion criteria for carious dentin substrate were that the caries lesion, surrounded by sound dentin, was limited to the occlusal surface and it was

extended at least half the distance from the enamel-dentin junction to the pulp chamber[6]. Molars were transversally sectioned (Isomet 4000, Buehler, Lake Bluff, IL, USA) at the mid-coronal portion of each tooth, to produce dentin discs (2.5 mm thick). Caries affected dentin surfaces surrounded by normal dentin were exposed and polished through SiC abrasive papers up to 4,000-grit with a final polishing procedure performed with diamond pastes (Buehler-MetaDi, Buehler Ltd.), through 1 μm down to 0.25 μm[15].

Then, specimens were divided into two halves by splinting the carious lesion, in order to obtain samples containing both areas of sound dentin and caries-affected dentin, in the same disc. The first half from each disc was destined to form the "untreated group" or "group before treatment". The second half was restored and kept in simulated body fluid solution (SBFS), pH 7.45, at 37 ºC, for 24 h. These specimens constituted the "treated group" or "group after treatment"[6]. The detailed composition of each amalgam is shown in Table 1. The specimens were, then, submitted to mechanical loading (100,000 cycles, 3 Hz, 49 N, for 9.2 h) (S-MMT-250NB; Shimadzu, Tokyo, Japan). Load cycling was repeated every seven days until completing a period of 3 w in SBFS storage (four load cycles, in total). To proceed with the mechanical loading, specimens were mounted in plastic rings using a dental stone. The cycling compressive load was applied using a 5-mm diameter spherical stainless steel plunger, while immersed in SBFS. The amalgam tiles were removed from the discs by cutting away the amalgam around the retentive pins. All specimens were submitted to X-Ray diffraction and transmission electron microscopy analyses, before amalgams placement (first half)/untreated group, and after amalgam removal (second half)/treated group.

2.2. X-Ray Diffraction (XRD) analysis.

The micro-X-ray diffractometer (μXRD[2]) used in this study was a single crystal diffractometer with a 2-dimensional detector system Cmos Photon 100 (Bruker-D8

Venture, Wien, Austria), equipped with kappa geometry based goniometer 2D Detector and XRD 2D Scan software. The X-ray beam (Cu Kα line, λ = 1.5418 Å) was generated by a Cu Microforms source Iμs and generator settings of 50.00 kV/1.00 mA were employed. The 2D position sensitive detector had 1024x1024 pixels. Both the starting and ending positions were: distance, 40.00 mm; 2θ: 40.00°; Omega: 20.00°; Phi: 270.00°; Chi: 50.00°. Wavelength of 1.54184 Å (Cu). The sample to detector distance was 40.00 mm, 2θ scanning angle range was from 10° to 80°. All measurements were performed at room temperature (295±0.1°K) and an exposure time: 60.00 s. A voltage of 50.00 kV, a current of 1.000 mA with the anode of Cu were used for the generator. For the detector, a frame size of 1024 pixels/ 98.30 mm, 104.17 pixels per centimeter in square shape were utilized. CuKα radiation was executed in $\theta-\theta$ scan. The tooth section was fixed to the sample holder. The XRD lines were identified by comparing the measured patterns to the JCPDS (Joint Committee on Powder Diffraction Standards) data cards[18].

From the micro-X-ray diffractometry pattern, the size of the crystallites, the root-mean-square of the lattice strain and the crystallites preferred orientation, were calculated. For this, it was proceeded as follows; first, by using Scherrer equation to calculate the crystallite size[3,19,20]:

$$d = \frac{K\lambda}{\beta \cos\theta} \qquad (1)$$

In this equation d is the mean size of the crystallites, K is a dimension less shape factor, with a value close to unite –note that in the case of dentin, $K \approx 0.94$ [3], and β is the peak full width at half maximum (FWHM) of the line broadening. Consequently, the broadening of the X-ray diffraction lines, in general, and the value of FWHM, in particular, are measurements of the crystallinity of a sample, this being more crystalline

the smaller the line broadening and the FWHM. Note, at this point, that crystallinity can be defined as the degree of structural order in a solid. Aimed to obtain the crystallite length and width, there was used this formula for the line broadenings corresponding to 002 and 310 reflections, respectively (Table 2).

Alternatively, the mean crystallite size, and also an estimation of the lattice strain, can be obtained by Scherrer-Wilson equation[3,19,21]:

$$\frac{\beta^2}{\tan^2\theta} = \frac{1}{d}\frac{K\lambda\beta}{\tan\theta\sin\theta} + 20\varepsilon_{rms} \qquad (2)$$

In this expression ε_{rms} is the root-mean-square of the lattice strain and, β, is the FWHM of the line broadenings. In order to obtain *d* from equation (2), it was calculated β and then plotted the values of $\frac{\beta^2}{\tan^2\theta}$ as a function of $\frac{K\lambda\beta}{\tan\theta\sin\theta}$ for the line broadening. The experimental data were approximately distributed along a straight line. Finally, there were obtained the slope and the intercept of the line of the best fit to the experimental data by performing a regression analysis using the method of least squares. From these data (slope and intercept) the crystallite size was obtained (equal to the inverse of the slope) and the root-mean-square of the lattice strain (equal to the intercept) –see Table 2. Note that the root-mean-square of the lattice strain is a measure of the local distortion of the lattice planes[22]. As for Scherrer equation, there were obtained the crystallite length and width by line broadenings corresponding to 002 (*H*) and 310 (*L*) reflections, respectively (see data in Table 2). In order to determine the interaction of variables with the HAp structure the ratio *H/L*[14] was calculated.

Finally, it was obtained the preferred orientation of the crystallites (texture) from the following intensity ratios[3]:

$$R_{hkl} = k_{hkl}\frac{I_{211}}{I_{hkl}} \qquad (3)$$

In this expression I_{211} and I_{hkl} are the intensities corresponding respectively to line reflections 211 and *hkl*, and $k_{hkl} = \frac{I_{hkl}^{st}}{I_{211}^{st}}$, where the superscript *st* refers to intensities calculated according to the JCPDS card. Note that *R* values close to unity correspond to random orientation, whereas *R* values significantly different than unity indicate the presence of preferred orientation of the crystallites in the crystallographic direction associated to the corresponding line reflection[3,23].

In order to assess the relative contribution of crystalline size and microstrain to the diffraction peak broadening, some selected samples were submitted to the Warren-Averbach analysis. This approach[21] was applied by using the software WinFit.

2.3. Transmission Electron Microscopy (TEM) analysis.

Samples were prepared following the protocol performed on bone[24]. This involved crushing the sample into a fine-grained powder in a liquid nitrogen mortar and pestle, and 2% NaOCl was added to remove the surrounding collagen, with daily changes for a week (using a sonicator). Small drops of ethanol were then placed on the power, followed by drawing the slurry into a micropipette. After washing with H_2O and ethanol, the nanocrystals were transferred to a 3 mm diameter carbon/Formvar coated cooper TEM grid. Before analysis, all samples were sputter coated with a thin layer of amorphous carbon. Electron lucent particles were selected by size and distant from grid bars. Stack images were acquired, and the position of the stage was changed between -40 and +50° of α tilt, and collected every 10º. The samples were analyzed using a Transmission Electron Microscope Zeiss Libra 120 (Oberkochen, Germany) at 120 kV in bright-field (BF), and selected area electron diffraction (SAED) modes. Normal BF images were produced by tilting the beam to the diffracting plane of interest.

Tomographic reconstructions and related data were proceeded with the software iTEM (Olympus Soft Imaging Solutions GmbH, Münster, Germany), comprising acquisition, alignment and visualization. A specific semi-automated modulus for image processing, attached to the microscope, including a 2048x2048 pixel chip BM-2k-120 Dual-Speed on axis SSCCD-camera (TRS, Moorenweis, Germany), was used. Series of images every 10º were collected, from -50 to +40. Rough images alignment were undertaken on a neighboring crystal, in order to minimize radiation damage. The obtained images were aligned and back projected using the software for 3D from the iTEM tomography extension. Reconstructions were obtained with a silicon graphics workstation self-incorporated.

3. Results and Discussion

Crystallites, with improved crystallographic orientation, became shorter and thinner in caries-affected dentin treated with Zn-containing amalgams, providing a local ion-rich environment with a relative lower lattice distortion.

Figures 1 to 4 are showing the refined μXRD^2 profiles attained in the experimental groups. TEM and SAED of the crystals are displayed in figures 5 to 9.

X-ray diffraction patterns of dentin indicate that they are constituted of HAp as a unique crystalline phase in both sound and caries-affected dentin after restoring with both Zn-free and Zn-containing amalgams restorations (Figs. 1 to 4).

3.1. Micro-X-ray diffraction pattern.

The analysis of μXRD^2 profiles of dentin showed that the physical broadening (FWHM) of peaks at 002 (2θ, 25.900º; centroid peak position θ_{hkl}, 0/0/-2; I, 10977386) reflection, after observing *data* plotted by the reduced full width and extended height at half maximum of the phosphate band, was increasing (~1.1 fold) in caries-affected dentin

surfaces restored with both Zn-free (Fig. 3) and Zn-containing (~1.0 fold) (Fig. 4) amalgams, after amalgam removal (Table 2). This lower sharp peaks or peak broadening[20] parallel to the *c*-axes[25] [002 plane] in the μXRD[2] (Table 2), indicated that a more amorphous dentin[26] with more crystals imperfections in nanocrystallite materials, *i.e.,* small crystallite size and lattice distortion[20] is produced. Similarly, peaks at 310 (2θ, 40.127º; centroid peak position θ_{hkl}, -3/1/0; I, 1380390) showed an increase of FWHM value (~1.2 fold) when Zn-free amalgam was used in caries-affected dentin surfaces (Table 2) (Fig. 3). In general, the narrower the spectral peak width is, the higher the degree of mineral crystallinity.

Diffractometry (Fig. 3) puts forward an almost complete overlapping in the range from 25.900º 2θ to 41º 2θ, corresponding to both analyses performed on caries-affected dentin surfaces before and after Zn-free amalgam placement. Reflection at 211 peak, and the diffraction ring corresponding to 211 and 112 planes (inset a, from Fig. 3), clearly establish the lower crystallinity after amalgam removal (inset b, from Fig. 3). The resulted broadening suggests the state of HAp as ultrafine nano-crystalline[27]. The association between broadening and poor crystallinity denotes the presence of, *i)* higher degrees of impurities and amorphous phase, with decreased chemical stability[26], and creates biogenic apatites that are characterized by low degree of crystallinity and non-stoichiometry[28]; and *ii)* increase in the crystal disorders of HAp, which has been linked to lower mechanical properties, likely related to increase solubility[23]. The broad peaks are usually attributed to the extremely small dimensions of the HAp crystallites, which is presumably due to the limited space available to intrafibrillar mineral. Broad diffractions peaks could also arise from weak long-range periodic correlations, or from crystal strain[5], as it will be discussed later. This poor crystallographic HAp is biological HAp that resulted after the incorporation of impurities such as carbonate, sodium and

magnesium ions[29]. It has been previously reported that the presence of magnesium, though negligible, within the lattice structure[30] produces a shortening of mineral crystallites[25]. Generally, the HAp with poor crystallinity has the better bioactivity, biocomopatibility and biodegradability as compared with the stoichiometric HAp. The dissolution of HAp increases the level of supersaturation, and thus increases the velocities of nucleation and growth of dentin-like apatite nanocrystals[29].

On the other hand, at 310 plane, a reduced FWHM value (~1.02 fold) was obtained when Zn-containing amalgams were employed (Table 2) (Figs. 2, 4), denoting an improved crystallographic or relative atomic order obtained from diffractometry, since narrower peaks suggest less structural variation in bond distances and angles[31]. In general, the narrower the spectral peak width is, the higher the degree of mineral crystallinity[32]. The analysis of μXRD^2 profiles confirmed higher intensities of caries-affected dentin surfaces after removal of Zn-containing amalgams at 002, 211 and 112 peaks, where diffractography patterns gradually transform from broad diffuse peaks before Zn-containing amalgams placement to sharper, more crystalline peaks after this amalgam removal (Fig. 4), confirming that amorphous phase itself is dynamic in nature. This also indicates that the mineral develops through some type of phase transformation process. This improved crystallinity may be due, in part, to the absence of Zn^{2+} and Sn^{2+} at the elemental X-ray detector system analysis. Both ions perform as Ca/P growth inhibitors[33], indicating destabilization of the amorphous state[34], favoring crystallinity at the new nucleated minerals[13].

On the contrary, reflections enclosed in the range from ~40º 2θ to 70º 2θ of traces involving the 310, 130, 113, 222, 213, 004, 304 and 143 peaks attained greater intensities before amalgams placement (Fig. 4).The analysis of μXRD^2 profiles comply with the depth profile 2-D μXRD^2 scan frames of caries-affected dentin before Zn-

containing amalgams placement (inset a, Fig. 4) and amalgam removal (inset b, Fig. 4) which showed continuous Debye-Scherrer rings at lower 2θ angles (40.00º). Similarly, the diffraction analysis formed brighter rings, after removal of Zn-containing amalgam, at 002 plane, in comparison to the caries affected dentin before amalgam placement, (inset a, Fig. 4), indicating lower line broadening of peaks, ~$3.5x10^2$ counts sharper after removal of Zn-containing amalgam in carious dentin (Fig. 4). TEM images of HAp, in bright-field (BF), exhibited polymorph/polyhedral or drop-like shaped crystals when caries-affected dentin was analyzed before Zn-containing amalgam placement (Figs. 8A, 8B), and were not transparent enough to observe their lattice, but stable enough for tilt series acquisition (Figs. 8A/B·I/II). Three-dimensional reconstructions of one of this particles displayed at different tilt angles permits to carefully examine the different local domains, and their alignment which compose this crystal. One view of the particle is insufficient to observe this phenomenon. The rounded drop-like shaped crystal (Fig. 5B) was confirmed to be more amorphous in nature than caries-affected dentin after removal of Zn-containing amalgams by its greater FWHM before treatment (0.0245) and the diffused ring pattern from the SAED analysis (top right inset, from Fig. 8B). Small spots and/or diffuse ring pattern indicate decreased crystallinity[17]. This faint electron diffraction halo, highlighted by the strong white dots, clearly shows, *i)* an image of the collagen matrix poor in minerals content[35], and *ii)* the simultaneous presence of crystalline phase, confirmed by the observation of some diffraction spots, immersed in an amorphous medium. The spontaneous formation of amorphous calcium phosphate in the presence or the organic matrix is a kinetically driven process[36]. *iii)* The faint preferred orientation (R*hkl*) that was observed (Table 2) might suggest that these apatite crystallites precipitated without any associated biologically controlled mineralization process[37]. In contrast, by the end of three weeks of load cycling, several

plate-shaped or needle-shaped micro-crystals arranged in layers (Figs. 9), isolates or attached to the grating, were depicted. Caries-affected dentin after Zn-containing amalgam removal was constituted mostly of tiny crystals of plate-shaped morphology (Fig. 9A, 9A·I), resulting beam sensitive. Beam damage appeared within several tens of seconds and caused the defragmentation of the crystallites. This might indicate that the material is composed of nanometer size crystallite flakes, which lost their mutual order under the radiation but did not disappear completely[38] (bottom left inset, from Fig. 9B). At variance, images obtained from this similar group, showed clustering of long and thin crystals (Fig. 9B), or platy or needle-like HAp crystals (Fig. 9C). Selected area electron diffraction (SAED) findings at an assembly of crystal polygons from figure 9A·I makes clear that the mineral phase is HAp, and it unveiled the (002) and (004) planes characteristic of bone and dentin (Fig. 9A·II)[5]. There is a gap in the ring just behind the (002) arc, because it is not really a powder ring, but three distinct sets of planes which have very close *d*-spacings[5]. The diffraction rings with diffused territories that were observed is a result of lower crystallinity, smaller crystallites size as well as the presence of organic material[15].

3.2. Crystallite size assessment.

The crystallite size, derived from Eqs. (1) and (2), is regarded as the size of the coherently diffracting domains, *i.e.*, coherent domain size is not limited to the grain sizes but may include imperfections (stacking faults, twins, dislocations arrays, or small-angle boundaries)[20]. The stacking or twin faults can introduce additional broadening and peak shifting[39]. It should be noted that the size of crystallites measures the volume-averaged size of the crystalline domains and not actual geometrical characteristics of the particles forming mineral phase of dentin[3]. A qualitative estimation of the size of the coherently scattering domain (*i.e.* the crystallite size) is

reported in Table 2, where an increase of the mean crystallite size (~1.0 fold) along a direction perpendicular to the *c*-axis [τ_{310} (*L*)] was obtained when caries-affected dentin surfaces were treated with Zn-containing amalgams. Crystallite size in calcified tissues has been shown to increase with tissue maturation[25,40]. Nevertheless, τ_{002} (*H*), related to the mean crystallite size along the *c*-axis[28] decreased (~1.0 fold) (Table 2); as a consequence, shorter but wider crystallites resulted after Zn-containing amalgam application on carious dentin (Table 2). Caries-affected dentin showed the shortest mineral crystallites (10.91nm), *i.e.*, the lesser needle shaped (decreased in average length) when Zn-containing amalgams were used for restorations, probably related to the incorporation of carbonate as substituent for PO_4^{-3} in the apatite lattice [25,41]. It is also speculated that zinc is expected to affect the crystal habit as well, since accommodation of this additional element within the crystalline structure of apatite (even in the interstitial position) could limit or decrease the growth rate in one or more directions, thus providing those reduced needle-like shape crystals (Figs. 9B, 9C)[38]. Therefore, taking into account the present results, it is possible to *i)* clearly associate both lower crystallinity and contraction along the direction orthogonal to the *c*-axis in caries-affected surfaces when Zn-containing amalgam restorations were used, and *ii)* to partially assume that the observed increasing degree of thickness of crystallites, in caries-affected dentin restored with Zn-containing amalgams (6.44 nm), fits with an increase in mineralization and maturity, as FWHM increased at τ_{310} (*L*) (Table 2). Apart from that, H/L ratio appeared slightly decreased for dentin treated with Zn-containing amalgam, 5.03% and 23.79 % in caries affected and sound dentin, respectively (Table 2). This finding suggests a weaker interaction of Zn-containing amalgams with the HAp structure[28] in sound dentin than in carious dentin. Nevertheless, crystallite thickness as determined by Scherrer equation has shown comparable width

data (5.88 nm and 4.68 in sound and carious dentin, respectively) with those obtained by Kinney et al. (2001)[42] who reported ~5.0 nm thickness.

It has been suggested that crystal growth is constrained in one axis, where concretely the thickness would be limited to the width of the 67-nm gap zone in the collagen fibril. This gap zone is primary site for apatite crystal nucleation and growth[42] crystallites of much lower crystallinity (0.0132) (Table 2). TEM pictures of sound dentin restored with Zn-free amalgams, in BF, ultimately exhibited needle-like crystals (Figs. 6H, 6I) of 11.23 and 5.84 nm at 002 and 310 reflections, respectively (Table 2). Those crystallites attained greater crystallinity after Zn-free amalgam restoration (Table 2) (Fig. 1), and became organized in pseudo-platelets of ~0.5 μm (Fig. 6I). Fig. 6G shows the outlines of the more well-defined domains superimposed on the -40º micrograph. Nevertheless, the lowest crystallinity, at both 002 and 310 planes, was precisely obtained by the sound dentin before amalgam restorations (0.0140 and 0.0329, respectively). This amorphization resulted associated to the lowest crystallite size, *H* and *L* values (10.64 nm and 4.68 nm, respectively), and so to the lowest grain size (10.37 nm and 4.40 nm, respectively) and the greatest microstrain ($4.75x10^{-4}$ and $2.54x10^{-4}$, respectively) (Table 2). All the observed crystallites put forward the same dominating morphological features of three-dimensional block-like and needle-like apatite crystals with outer contours of spike and start-like shapes (Fig. 7). Relevant to this morphology, micron size crystallites had thin wedge-like edges and allowed the study of the electron diffraction pattern (top right inset, from Fig. 7B). This bright-field TEM image complied with an electron diffraction pattern which indicates that the structure of the crystal is amorphous (halo rings) and crystalline (diffraction spots), in part.

3.3. Grain size assessment.

The ultra-structural observations confirmed that the grain size, expressed throughout the Scherrer-Wilson equation (Eq. 2) of dentin crystals became smaller in caries-affected dentin restored with both Zn-free amalgams (~1.09 fold) and Zn-containing amalgams (~1.03 fold) at 002 reflections (Table 2). On the contrary, at 310 reflections, the grain size augmented (~1.02 fold) after treating the caries-affected dentin substrate with Zn-containing amalgam. Grain size and lattice microstrain accordingly can be determined by assessing the deviation of line profile from perfect crystal diffraction[20].

3.4. Microstrain assessment.

Microstrain (Eq. 2) was measured as the change in *d*-spacing of a strained sample compared to the unstrained state of a perfect or standard crystal[25], and calculated from 002 and 310 was tensile for all crystallites, in dentin. The lattice strain within the long dimension (002 reflection) of the dentin crystals, in caries-affected dentin restored with Zn-containing amalgam, increased ~1.06 fold, respect to the untreated group, but decreased ~1.19 fold when Zn-free amalgams were used and compared with the untreated group (Table 2). Caries-affected dentin before Zn-free amalgam treatment proved the largest and characteristic crystallites with needle-like morphology, in bright-field TEM images. Those crystallites formed platelets of micron size (Fig. 5A), resulting also beam sensitive. The predominant ring pattern corresponding to 002 planes appearing in form of two semi-circles instead of a continuous ring (Fig. 5B) indicate that the crystallites have preferred orientation in *c*-direction[43]. Indexes and *d* values calculated (Fig. 5B) are in good agreement with the hexagonal structure of HAp[38]. Most strain was concentrated in caries-affected dentin restored with Zn-containing amalgams (4.52×10^{-6}) (Table 2). These increased strain values accounted for the broadening of diffraction peaks (0.0136) even in the presence of the lowest grain size (10.63 nm)[28] and

the precise difference of intensity counts in the μXRD^2 analysis at 002 reflection (~3 x 10^2) and 211 reflection (~9 x 10^2) (Fig. 2). At 310 reflections, caries-affected dentin restored with Zn-containing amalgams gave rise to a 4.97 % reduction in microstrain, and to an increase in both grain (2.31%) and crystallite size (2.18%), in comparison with the untreated group (Table 2). The different mean crystallite sizes obtained are essentially due to the contribution of the strain to the broadening of the diffraction peaks[28]. Relative to this, a peak broadening may be a result of a significant organic fraction in dentin[40], characteristic of caries-affected dentin substratum[44]. Nano-sized crystallites normally show high surface energy, which increases with the reduction of the size of the crystallites and therefore results in the presence of uniform and nonuniform strain in the particles[3]. Broadening of peaks and dissolution of crystals resulted to be associated. Dissolution of crystal planes with higher energies is more favorable to reduce the surface energy, contributing to mineral re-precipitation preferentially in the *c*-axis, carrying out a good *in vitro* bioactivity [45].

3.5. Texture assessment.

Texture is the distribution of crystallographic orientation of a polycrystalline sample, it accounts for changes in microstructure, proving a great influence on materials properties, as cracking resistance[46]. Texture indices (R_{hkl}) in dentin polycrystalline structures were calculated according to Eq. (3). For $R \approx 1$, the grains were considered randomly oriented[3]. This criterion was only followed by the group of caries-affected dentin restored with Zn-free amalgams (R_{hkl}= 0.994) (Table 2), at the 002 plane; thereby, this group did not hardly ever show any distinct texture[46]. *R* values greater or lower than 1.0 indicate the presence of preferred grain orientation or texture[23]. The degree is dependent on the percentage of crystals having the preferred orientation[46]. A*R* rising (~1.13 fold) was achieved by the carious dentin restored with Zn-containing

amalgams (Table 2). After SAED analysis (Fig. 9A·II), it can be assumed that the appearance of the spotty rings without preferred orientation and these three planes simultaneously, indicates that there is more than one orientation of the HAp platelets in the plane[5,15]. Fig. 9C implicitly reveals, in BF, that crystals are composed of domains of locally oriented crystal arrays, showing a well-defined lineation. Carious dentin before restoration (Fig. 5A), comparatively, showed different oriented diffraction pattern. As the *c*-axes of the crystals are aligned with the collagen fibrils, it may be inferred from the above observations that in particles with oriented diffraction patterns all the collagen fibrils have the same orientation, but the crystal layers in different fibrils are not aligned with respect to one another[2]. The fact that the mineralized collagen fibrils in the neighboring domains have different orientation accounts for the electron diffraction pattern of the particle not displaying an overall preferred c-axis alignment[2]. This different alignment was more explicitly appreciated in the bright-field TEM relative to dentin before restoration (Fig. 7), where crystals followed perpendicular orientation respect to one another, illustrating that they are composed of locally ordered domains. The crystals in each domain have essentially the same organization as those found in collagenous matrices; thus, they are composed of domains that have the same basic crystal organizational structure as those with oriented electron diffraction patterns[2].

Sound and caries-affected dentin treated with Zn-free amalgams attained, at 310 reflections, texture indices greater than 1 (1.320 and 1.238) (Table 2), which put emphasis on the preferred orientation of the crystallites in the crystallographic direction, at these planes[3,23] exhibiting a perpendicular alignment to the occlusal surface, as *R* values are greater than 1.0[23]. On the contrary, at the reflections 002 all assessments resulted lower than 1.0 ($R<1$), but all groups showed less variation than at 310 reflection, *i.e.,* less nano-degradation for the former[23]. As *R* values are less than 1.0,

crystallites are aligned parallel to the occlusal surface[23]. In addition, the scarce variation of *R* values within this reflection mode 002 suggests the existence of a modest gradation in texture at the nanometer scale within the complex dentin microstructure. This means poor three-dimensional interlocking HAp structure to withstand strength and provide both hardness and stress-bearing capability[23]. From the results described above, it appears that the degree of crystal disorder in HAp may be related to its crystal size.

It has been further proposed[23] that the degree of hydroxylation or the incorporation of OH^- within the HAp decreases as the crystal size decreases. A lack of OH^- in nanocrystalline HAp is believed to cause crystal disorder. OH^- ions are more readily incorporated into apatites with a large crystal lattice which induces the polar nature of the HAp. Polarity is crucial for the high degree of alignment of crystallites. This lack of both OH^- and polarity is believed to result in their random alignment and thus a high degree of crystal disorder. It appears that nature imposes a specific state of crystal disorder by varying the concentration of OH^- to enhance the ability of biological apatites to carry out their tissue-specific functions[47]. Therefore, the hydroxyl groups in the HAp can act as active sites for the nucleation of dentin-like apatites[45].

It is important to place emphasis on that amorphous calcium phosphate provides a local ion-rich environment which is considered favorable for *in situ* generation of prenucleation clusters, succeeding further dentin remineralization[48]. On the contrary, if crystalline calcium phosphates are formed, they will have long degradation times, requiring months or even years to provide ions to the remineralizing media[49]. The biodegradability of these new mineral formations depends on many parameters such as crystallinity, porosity, chemical purity, surface roughness, pH in the media, and other solubilized ions present at the oral environment[33,50]. Two reasons may be, then, advocated to justify the structural observations that crystallites were becoming smaller

and thinner in caries affected dentin treated with Zn-containing amalgams, *i)* the special role of the *in vitro* transferred waves of mastication into coronal dentin[3], which promoted lattice distortion after mineral crystallization on amorphous nuclei on the partially demineralized dentin[13], and *ii)* the presence of Zn and other impurities at the restorative interface[51]. Zn^{2+} inhibits HAp crystal growth. The substitution for calcium occurs up to about 20 atom%, whereas the apatite structure does not sustain higher Zn^{2+} incorporation. The substitution of zinc into HAp resulted in a decrease of both *a*- and *c*-axes of the unit cell, consistent with the smaller ionic radius of Zn^{2+} with respect to Ca^{2+}[52]. A correct evaluation of cell parameters at relatively high zinc content are hindered by the progressive broadening of the XRD peaks, due to the reduction of crystal sizes and/or the increase of crystal strain with increasing Zn^{2+} concentration[53]. Nevertheless, even when the crystallinity of the inorganic phase is high, it is difficult to find direct evidence of ionic substitution, also because the degree of replacement is always relatively low[53].

These are, to the best of our knowledge, the only available results from both μXRD[2] and TEM/SAED combined methodologies relevant to analyze sound and caries-affected dentin submitted to amalgam restorations. Thereby, this investigation represents the first attempt to assess the crystal ultrastructure of sound and carious dentin mineral phase, and interpret its morphology before and after amalgam restorations. These outcomes are important, because they provide information on bio-physic-chemical structure of dentin treated with amalgam, for essential clinical applications. Relative to complementary experimental techniques that ultimately illustrate the clinical answer of sound and carious dentin, dark-field TEM (DF-TEM), High Resolution TEM (HRTEM) and Scanning Transmission Electron Microscopy (STEM) should be incorporated into our methodology, for future strategies of research.

Nevertheless, our study also has several weakness; longer duration of mechanical loading even exploring some *in vitro* para-functional habits as bruxism, would have expanded the message of this paper, and should have been considered. Future works will also include determining the diffusion of matrix damage and the assessment of visible microcraks. These represent topics for further research. Moreover, these approaches open up the possibility of future probing of other materials-tooth interfaces, *e.g.*, resin-based adhesives and glass-ionomer cements, as well as extending the assessments to other hard tissues as enamel, cementum and bone. Furthermore, once characterized these new crystals that appeared at the carious dentin surface after Zn-containing restorations load cycled, it might be interesting to develop new composites based on this hydroxyapatite, by bio-monitoring these data. Applying advanced technologies, both biofunctionality and biocompatibility studies should be carried out by using these starting crystals for the production of hydroxyapatite for therapeutic dental applications in regions of demineralized dentin. This approach also deserves future research.

4. Conclusions

1. Crystallinity decreased in caries-affected dentin surfaces when treated with Zn-containing amalgams, at 002 reflection. This amorphization provided an ion-rich environment, favorable for *in situ* dentin remineralization, as it resulted associated to both the lowest crystalline and grain size, and greatest microstrain.

2. Crystallinity increased in caries-affected dentin surfaces treated with Zn-containing amalgams, at 310 reflection, thus providing long degradation times, hindering the physio-pathological dentin repair processes.

3. Shorter but wider crystallites resulted after Zn-containing amalgam application on carious dentin, thus increasing mineralization and maturity.

4. Caries-affected dentin treated with Zn-free amalgams was characterized by grains that were considered randomly oriented, and caries-affected dentin treated with Zn-containing amalgams showed preferred grain orientation or texture.

5. The scarce gradation in texture within the dentin microstructure at 002 reflection results associated to poor three-dimensional interlocking of the hydroxyapatite structure to withstand strength and provide both hardness and stress-bearing capability.

Acknowledgements

This work was supported by grants MINECO/FEDERMAT2014- 52036-P and FIS2013-41821-R. The authors have no financial affiliation or involvement with any commercial organization with direct financial interest in the materials discussed in this manuscript. Any other potential conflict of interest is disclosed.

References

1. C. Xu and Y. Wang, *Arch. Oral Biol.*, 2012, **57**, 383.
2. S. Weiner, W. Traub and H.D. Wagner, *J. Struct. Biol.*, 1999, **126**, 241.
3. J. Xue, A.V. Zavgorodniy, B.J. Kennedy, M.V. Swain and W. Li, *J. Microsc*., 2013, **251**, 144.
4. A.V. Zavgorodniy, R. Rohanizadeh and M.V. Swain, *Arch. Oral Biol.*, 2008, **53**, 124.
5. M.J. Olszta, X. Cheng, S.S. Jee, R. Kumar, Y.Y. Kim, M.J. Kaufman, E.P. Douglas and L.B. Gower, *Mater. Sci. Eng. R. Rep*., 2007, **58**, 77.
6. M. Toledano, F.S. Aguilera, E. Osorio, I. Cabello, M. Toledano-Osorio and R. Osorio, *Biointerphases*, 2015, 031002.
7. R. Osorio and M. Toledano, in *Biomineralization and Biomaterials,* ed. C. Aparicio and M. Pau Ginebra, Woodhead Publishing series in Biomaterials: Number 104. Elsevier, Cambridge, UK, 1st edition, 2016, Biomaterials for catalysed mineralization of dental hard tissues, pp. 365-374.
8. L. Bjørndal and A. Thylstrup, *Eur. J. Oral Sci*., 1995, **103**, 25.
9. N.J. Opdam, E.M. Bronkhorst, B. A. Loomans and M.C. Huysmans, *J. Dent. Res.*, 2010, **89**, 1063.
10. N. Donmez, S. Belli, D.H. Pashley and F.R. Tay, J. Dent. Res., 2005, **84**, 355.
11. P. Spencer, Q. Ye, A. Misra, S.E.P. Goncalves and J.S. Laurence, *J. Dent. Res.,* 2014, **93**, 1243.
12. K. Anusavice, *Phillips' Science of Dental Materials*, ed. Saunders, Elsevier, St. Louis, MO, 11th ed., 2003, p. 832.
13. M. Toledano, F.S. Aguilera, E. Osorio, M.T. López-López, I. Cabello, M. Toledano-Osorio and R. Osorio, *Biointerphases,*2015, **10**, 041004.

14. A. Bigi, E. Boanini, B. Bracci, G. Falini and K. Rubini, *J. Inorg. Biochem*., 2003, **95**, 291.
15. J.H. Lee, H. Kim, T. Kim, J.H. Song, W.S. Kim and J. Ham, *Bull. Korean Chem. Soc.,* 2013, **34**, 42.
16. E. Filippo, C. Carlucci, A.L. Capodilupo, P. Perulli, F. Conciauro, G.A. Corrente, G. Gigli and G. Ciccarella, *Mater. Res.*, 2015, **18**, 473.
17. F. Wang, E. Guo, E. Song, P. Zhao and J. Liu, *Adv. Biosci. Biotech*., 2010, **1**, 185.
18. International Centre for Diffraction Data, 2005, Powder Diffration File 09-0432.
19. F. Perales, C. De las Heras and F. Agulló Rueda, *J. Phys. D: Appl. Phys.,* 2008, **41**, 225405.
20. Z. Zhang, F. Zhou and E.J. Lavernia, *Metall. Mater. Trans*., 2003, **34A,** 1349.
21. H.P. Klug, and L.E. Alexander. *X-Ray Diffraction Procedures: For Polycrystalline and Amorphous Materials*, John Wiley & Sons, New York, 2nd Edition, 1974.
22. D. Lewis and D.O. Northwood, *Strain*, 1968, **4**, 19.
23. I.M., Low, *J. Am. Ceram. Soc*., 2004, **87**, 2125.
24. S. Weiner and W. Traub, in *Mechanisms and Phylogeny of Mineralization in Biological Systems,* eds. S. Suga and H. Nakahara, Springer-Verlag, New York, 1991, Organization of crystals in bone, p. 247.
25. R.G. Hanschin and W.B. Stern, *Bone*, 1995, **16**, 355S.
26. A. Moshaverinia, S. Ansari, M. Moshaverinia, N. Roohpour, J.A. Darr and I. Rehman, *Acta Biomater*., 2008, **4**, 432.
27. Y. Liu, J. Huang and H. Li, *J. Mater. Chem. B*., 2013, **1**, 1826.

28. A. Bigi, E. Boanini, M. Gazzano, M.A. Kojdecki and K. Rubini, *J. Mater. Chem.*, 2004, 14, 274.
29. C. Chen, J. Liu, F. Sun and J.W. Stansbury, *RSC Adv.*, 2014, **4**, 28928.
30. M. Toledano, F.S. Aguilera, M.T. López-López, E. Osorio, I. Cabello, M. Toledano-Osorio and R. Osorio, *J. Mech. Behav. Biomed. Mater.*, 2016, In press.
31. A.G. Schwartz, J.D. Pasteris, G.M. Genin, T.L. Daulton, and S. Thomopoulos, *PloS One*, 2012, **7**, e48630.
32. K. Karan, X. Yao, C. Xu and Y. Wang, *Dent. Mater.*, 2009, **25**, 1205.
33. A. Hoppe, N.S. Güldal and A. R. Boccaccini, *Biomaterials*, 2011, **32**, 2757.
34. F. Barrére, P. Layrolle, C. A. van Blitterswijk and K. de Groot, *Bone,* 1999, **25**, 107S.
35. Y. Chen, J. Wang, J. Sun, C. Mao, W. Wang, H. Pan, R. Tang and X. Gu, *J. Mech. Behav. Biomed. Mater*., 2014, **40**, 297.
36. S. Gajjeraman, K. Narayanan, J. Hao, C. Qin and A. George, *J. Biol. Chem.*, 2007, **282**, 1193.
37. A.V. Zavgorodniy, R. Rohanizadeh, S. Bulcock and M.V. Swain, *Acta Biomater*., 2008, **4**, 1427.
38. I. Mayer, F.J.G. Cuisinier, S. Gdalya and I. Popov, *J. Inorg. Biochem.*, 2008, **102**, 311.
39. C.N.J. Wagner, in *Local Atomic Arrangements Studied by X-ray Diffraction,* ed. J.B. Cohen and J.E. Hilliard, New York: Gordon and Breach, 1966, chapter 6.
40. H. Gawda, L. Sękowski and H. Trębacz, *Biomechanics*, 2004, **6**, 41.
41. M. Toledano, E. Osorio, F.S. Aguilera, I. Cabello, M. Toledano-Osorio and R. Osorio, *J. Biomed. Optics,* 2016. In press.

42. J.H. Kinney, J. Oliveira, D.L. Haupt, G.W. Marshall and S.J. Marshall, *J. Mater. Sci. Mater. Med.*, 2001, **12**, 743.

43. L.D. Landau and E.M. Lifshitz, *Statistical Physics (Part 1)*, 3rded, Butterworth-Heinenann Ltd., Oxford, 1980.

44. G.W. Marshall Jr., S.J. Marshall, J.H. Kinney and M. Balooch, *J. Dent*., 1997, **25**, 441.

45. X.Y. Cheng, X.Q. Chen, D.Z. Li and Y.Y. Li, *Acta Crystallogr. C. Struct. Chem.*, 2014, **70**, 85.

46. K.D. Liss, A. Bartels, A. Schreyer and H. Clemens, *Text. Microstruct.*, 2003, **35**, 219.

47. J.D. Pasteris, B. Wopenka, J.J. Freeman, K. Rogers, E. Valsami-Jones, J.A.M. van der Houwen and M.J. Silva, *Biomaterials*, 2004, **25**, 229.

48. Y. Liu, L. Tjaderhane, L. Breschi, A. Mazzoni, N. Li, J. Mao, D.H. Pashley and F.R. Tay, *J. Dent. Res*., 2011, **90**, 953.

49. K. Rezwan, Q.Z. Chen, J.J. Blaker and A.R. Boccaccini, *Biomaterials*, 2006, **27**, 3413.

50. N.J. Cochrane, F. Cai, N.L. Huq, M.F. Burrow and E.C. Reynolds, *J. Dent. Res.* 2010, **89**, 1187.

51. M. Toledano, F.S. Aguilera, E. Osorio, I. Cabello, M. Toledano-Osorio and R. Osorio, *Microsc. Microanal.*, 2015, **21**, 214.

52. A. Bigi, E. Foresti, M. Gandolfi, M. Gazzano and N. Roveri, *J. Inorg. Biochem.*, 1995, **58**, 49.

53. Bigi A, Boanini E, Gazzano M. in *Biomineralization and Biomaterials*, ed. C. Aparicio and M. Pau Ginebra, Woodhead Publishing series in Biomaterials:

Number 104. Elsevier, Cambridge, UK, 1st edition, 2016, Ion substitution in biologicaI and synthetic apatites. p. 236.

Legend of figures.

Figure 1. Refined μXRD^2 profiles of sound dentin before Zn-free amalgam placement and after the removal of the restoration. The corresponding Debye-Scherrer rings are shown in inset a (before amalgam placement) and b (after amalgam removal). Vertical bars represent HAp peaks.

Figure 2. Refined μXRD^2 profiles of sound dentin before Zn-containing amalgam placement and after the removal of the restoration. The corresponding Debye-Scherrer rings are shown in inset a (before amalgam placement) and b (after amalgam removal). Vertical bars represent HAp peaks.

Figure 3. Refined μXRD^2 profiles of caries-affected dentin before Zn-free amalgam placement and after the removal of the restoration. The corresponding Debye-Scherrer rings are shown in inset a (before amalgam placement) and b (after amalgam removal). Vertical bars represent HAp peaks.

Figure 4. Refined μXRD^2 profiles of caries-affected dentin before Zn-containing amalgam placement and after the removal of the restoration. The corresponding Debye-Scherrer rings are shown in inset a (before amalgam placement) and b (after amalgam removal). Vertical bars represent HAp peaks.

Figure 5. Bright-field of an assembly of faint needle-like apatite crystals of caries-affected dentin treated with Zn-free amalgam, before the restoration placement (A). The arrows show the predominant direction of the *c*-axes. The pointers show the cut domains with the sectioned crystals seen face-on. B shows a selected area electron

diffraction (SAED) of the crystals (+) observed in (A), at nanoscale. It depicts a relative diffuse halo ring, indicating some amorphous structure and clear diffraction spots, indicating the presence of remnant crystallite matter.

Figure 6. Bright-field of an assembly of needle-like apatite crystals of caries-affected dentin treated with Zn-free amalgam, after the restoration removal (A) and (H). The collage shows views at different tilt angles after tomographic reconstructions, at 0º (B), 20º(C), 50º(D), -20º(E), and -40º (F), from A. G shows that the particle have multiple domains of locally aligned crystal arrays. I, Magnified observation of a section from (H), showing the needle-like appearance of crystallites.

Figure 7. Bright-field of an assembly of block-like and needle-like apatite crystals of sound dentin before restoration with Zn-containing amalgam (A). B, Crystals followed perpendicular alignment respect to one another (arrow and pointer). B also shows a selected area electron diffraction (SAED) of the crystals (+) shown in (A), at nanoscale. The collage shows views at different tilt angles after tomographic reconstructions, at 10º(C), 50º(D), -10º(E) and -30º(F). The particles have any domain of locally aligned crystal arrays.

Figure 8. Bright-field of an assembly of polyhedral (A) or rounded (B)/drop-like shaped crystal of caries-affected dentin before Zn-containing amalgam placement; the inset at B at microscale, (+), presents small spots and diffused ring pattern, indicating the existence of low degree crystalline nano-phase. The collages I and II show views at different tilt angles after tomographic reconstruction, at 40º(A·I), -20º(A·II), 20º(B·I)

and -30º(B·II). Comparison of the images shows that the particle has any domain of locally aligned crystal arrays.

Figure 9. Bright-field of an assembly of plate-like polygons (A) and three-dimensional agglomerated crystals (B) of caries-affected dentin after Zn-containing amalgam removal. The bottom left inset represents the beam damage under the radiation. A·I represents, at big magnification, the staggered order of those plate-like crystallites. A·II shows a selected area electron diffraction (SAED) of the crystals (+) shown in (A) at microscale; it exhibits the sharp 002 diffraction peak reflecting the elongated nature of the crystals, a first broad diffraction band containing 211 and 112 grouped peaks, and a second broad diffraction band containing 130, 113, 222, and 004 peaks. It confirms the presence of hexagonal apatite and a highly polycrystalline structure at the characteristic scale of 1 μm. C, Needle-like crystals were also observed, with crystallites seen as plates when viewed face-on. The arrows show the predominant direction of the c-axes.

FIGURE 1

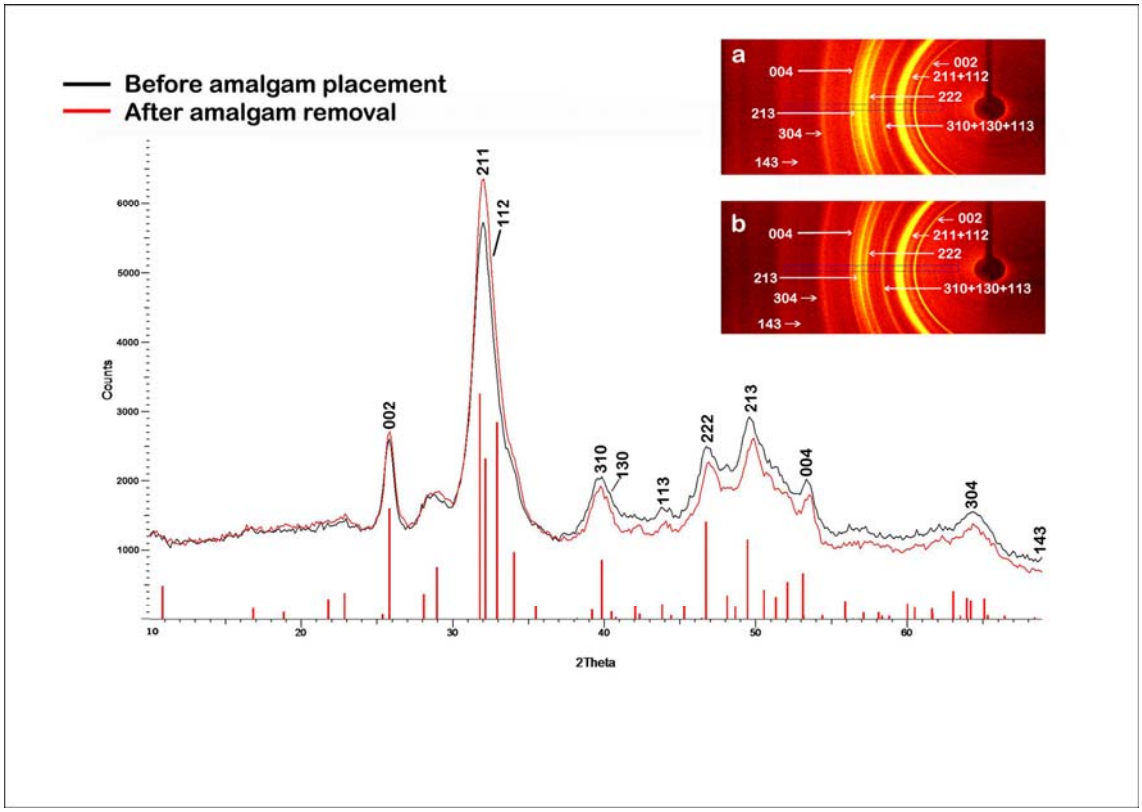
Before amalgam placement
After amalgam removal
a
004
002
211+112
222
213
304
310+130+113
143
b
004
002
211+112
222
213
304
310+130+113
143
Counts
2Theta
002
211
112
310
130
113
222
213
004
304
143

FIGURE 2

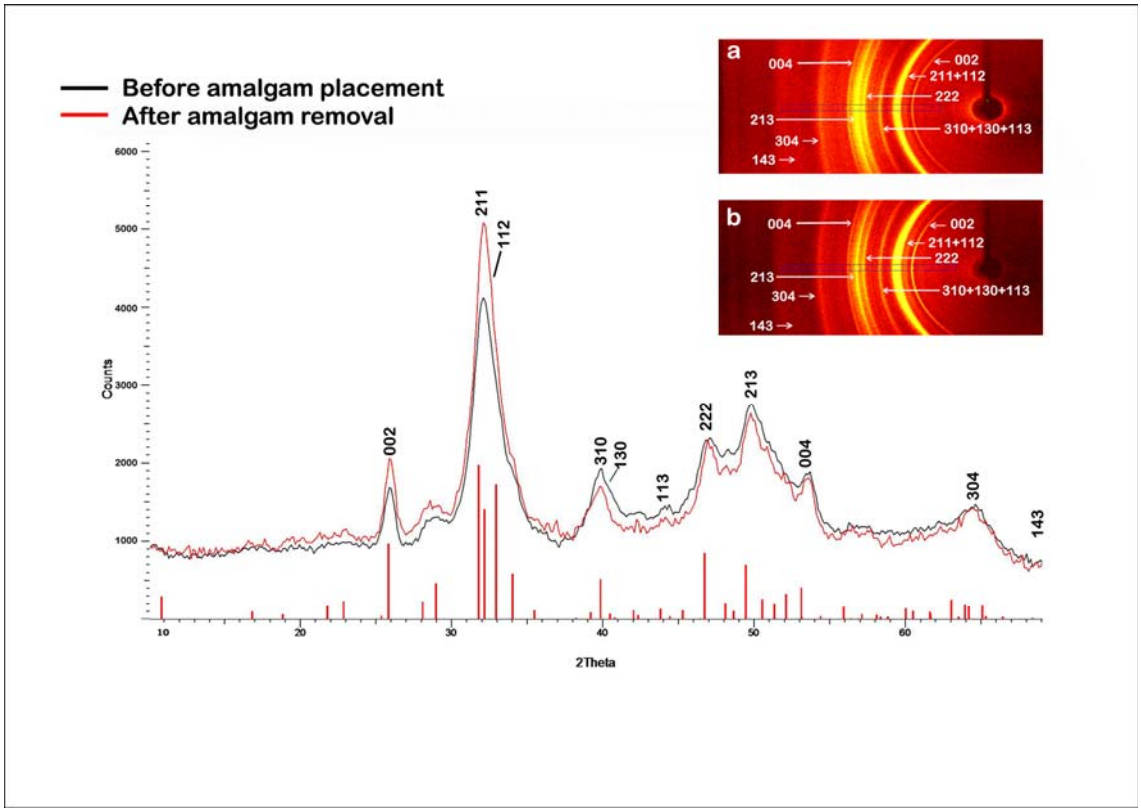
Before amalgam placement
After amalgam removal
a
004
002
211+112
222
213
310+130+113
304
143
b
004
002
211+112
222
213
310+130+113
304
143
Counts
2Theta
002
211
112
310
130
113
222
213
004
304
143

FIGURE 3

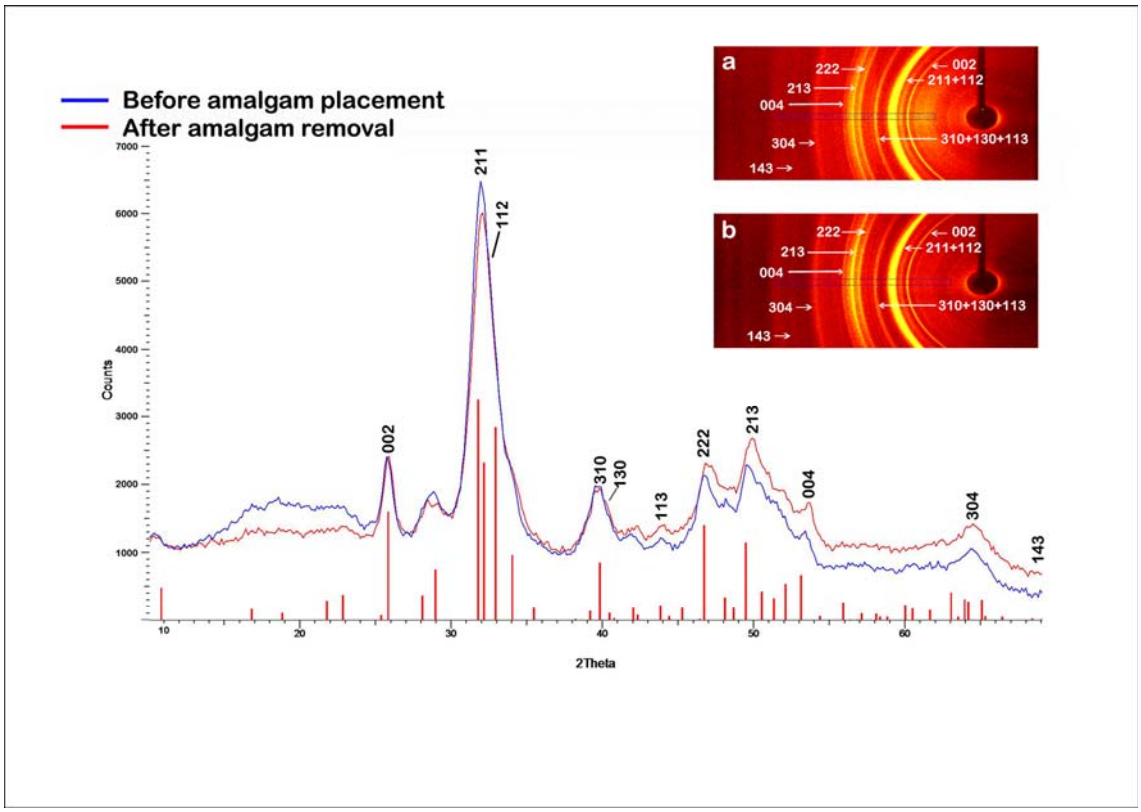
Before amalgam placement
After amalgam removal
a
b
222
213
004
304
143
002
211+112
310+130+113
Counts
2Theta
211
112
002
310
130
113
222
213
004
304
143

FIGURE 4

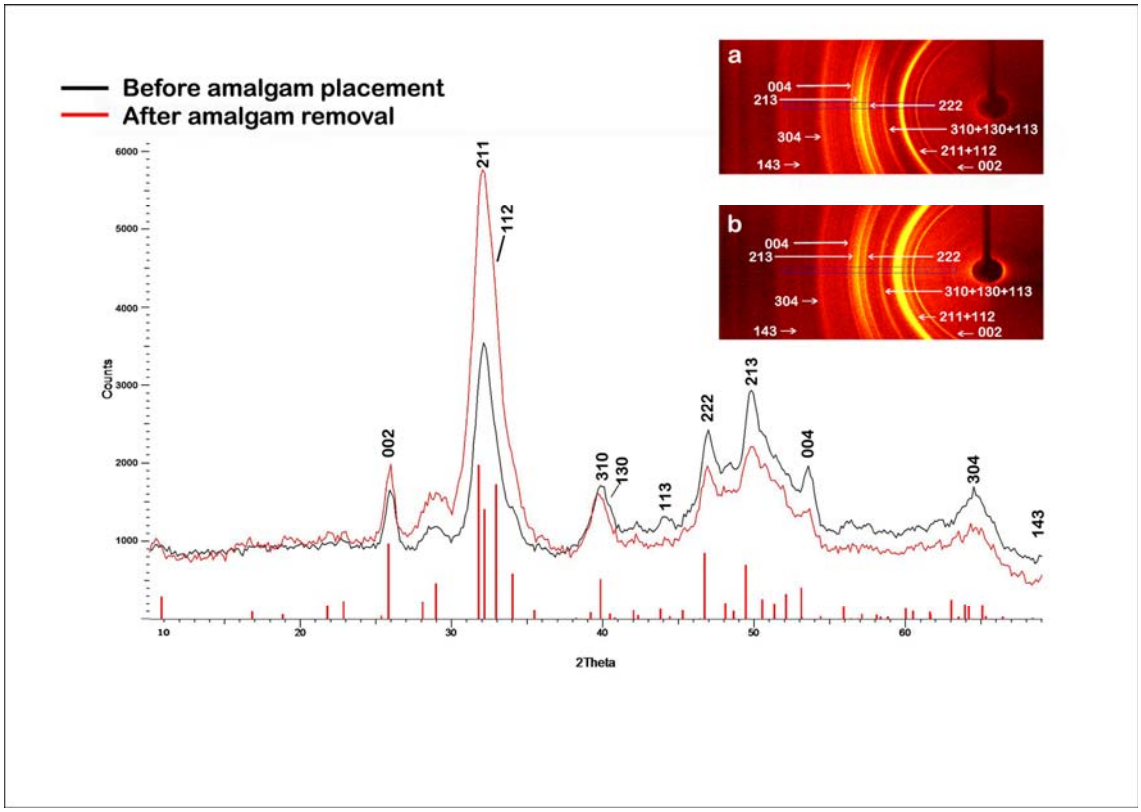
Before amalgam placement
After amalgam removal
a
004
213
222
310+130+113
304
211+112
143
002
b
004
213
222
310+130+113
304
211+112
143
002
Counts
2Theta
002
211
112
310
130
113
222
213
004
304
143

FIGURE 5

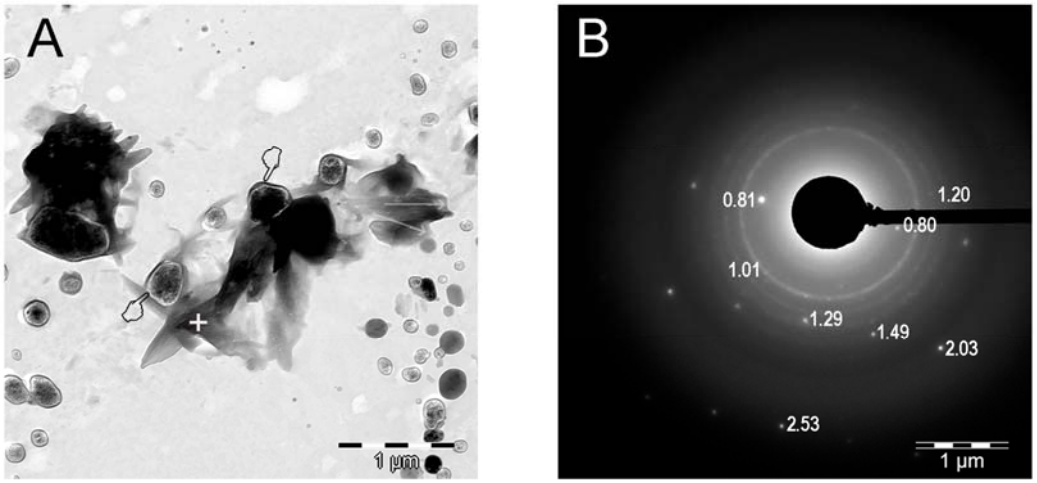

FIGURE 6

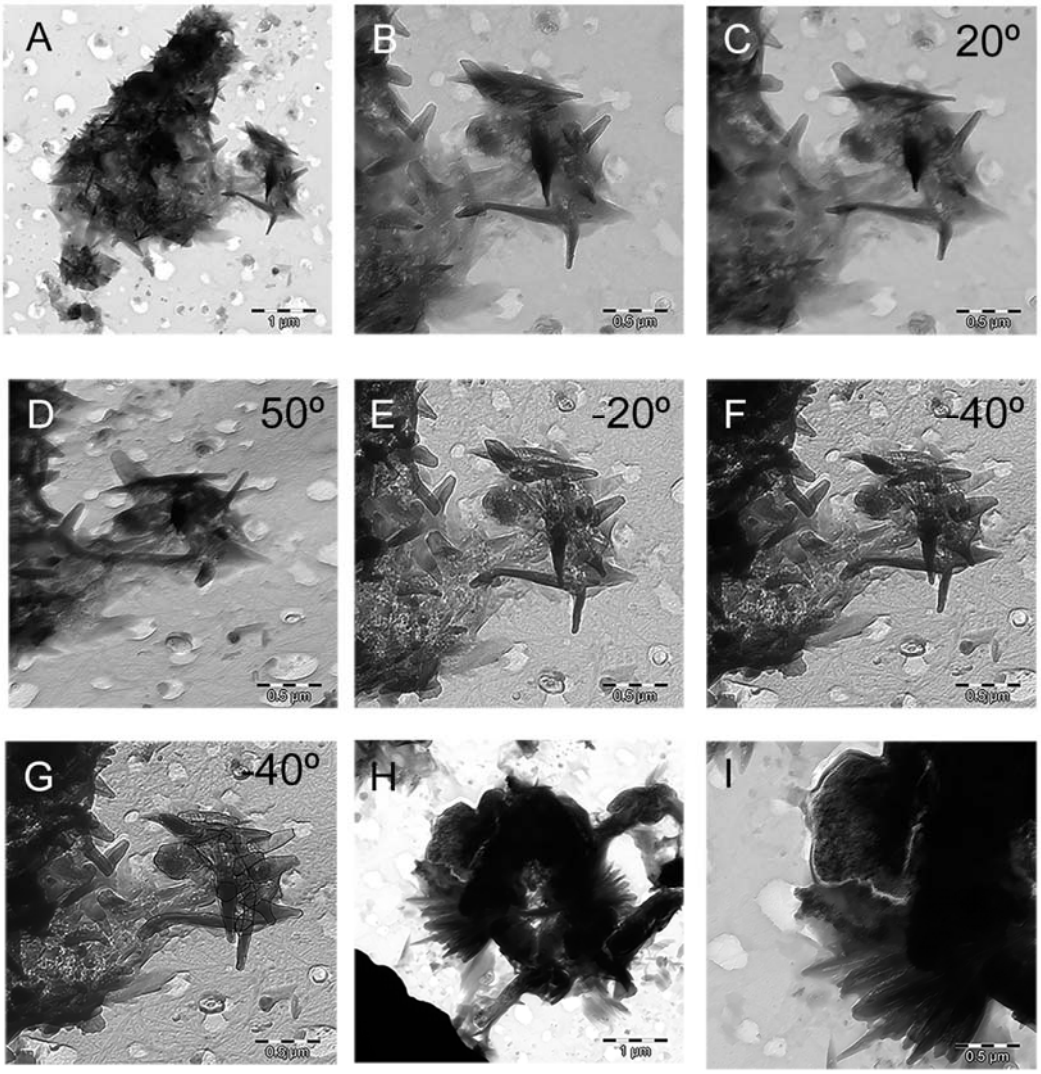
A
1 µm
B
0.5 µm
C
20º
0.5 µm
D
50º
0.5 µm
E
-20º
0.5 µm
F
-40º
0.5 µm
G
-40º
0.5 µm
H
1 µm
I
0.5 µm

FIGURE 7

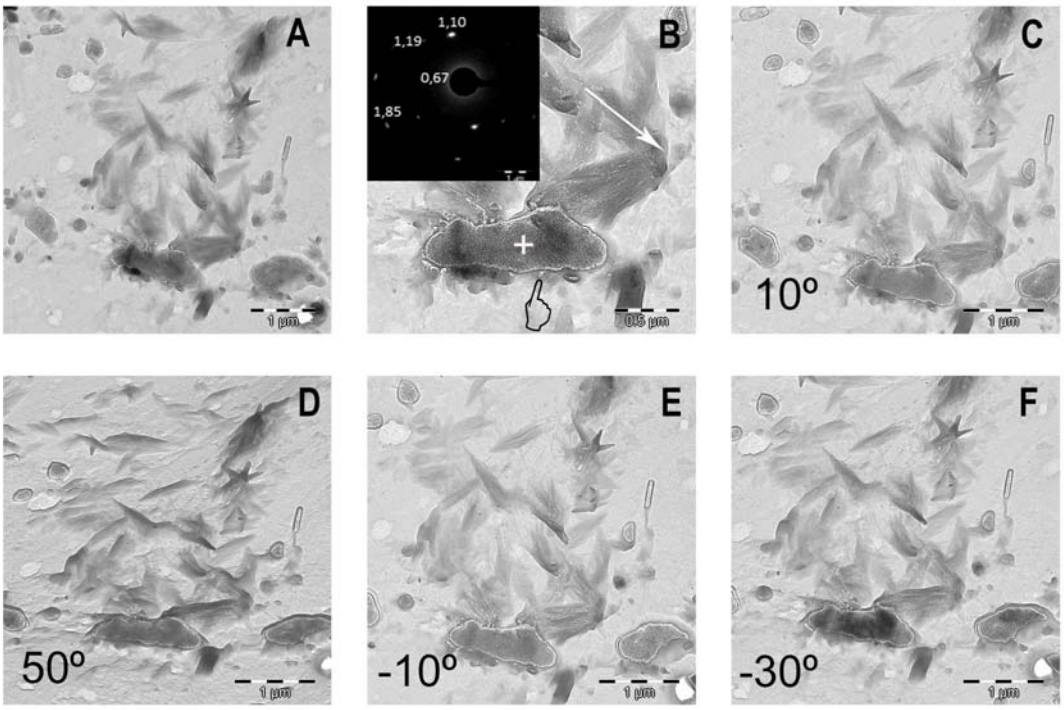

FIGURE 8

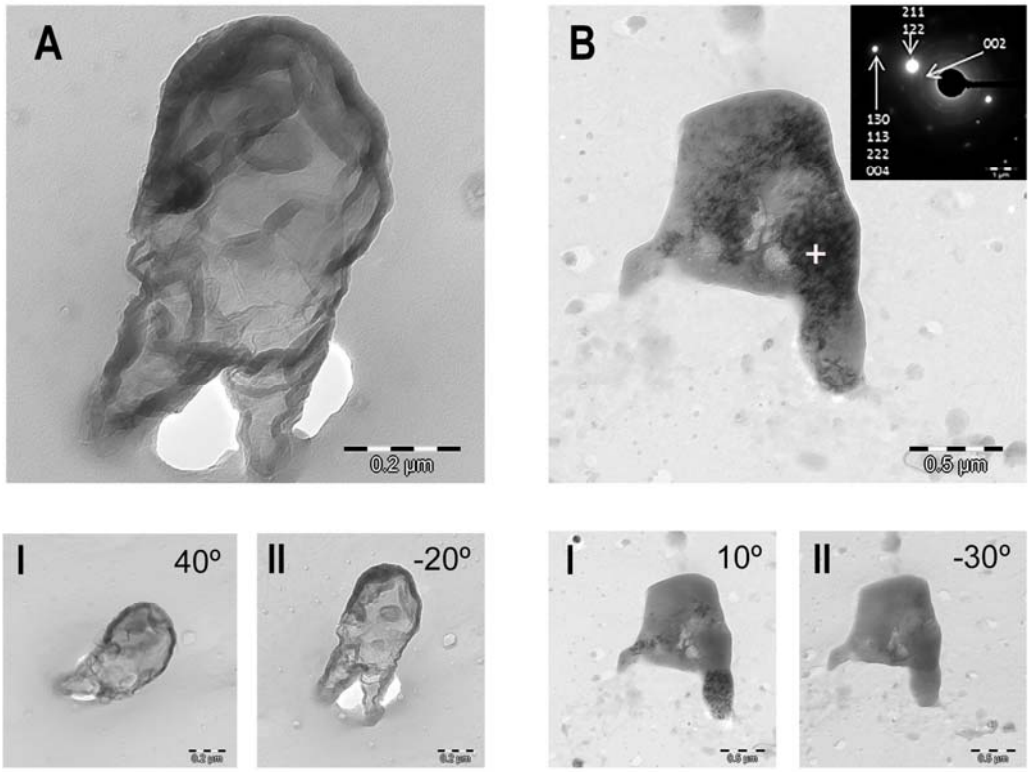

FIGURE 9

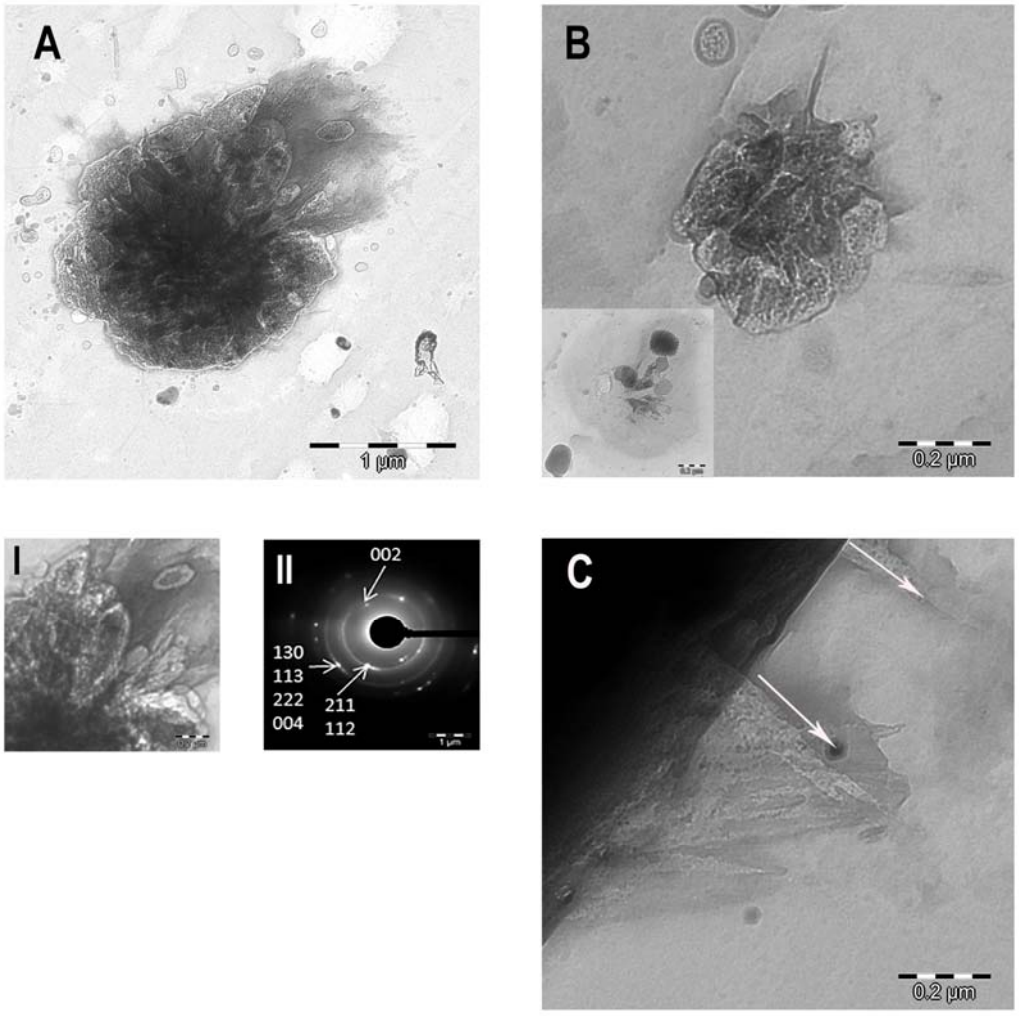

Table 1. Composition of amalgams used in the present study.

AMALGAM	COMPOSITION	
	Alloypowder	**Weight %**
Megalloy EZ®* (Zn-free)	Silver	56.7 %
	Tin	28.6 %
	Copper	14.7%
The recommended alloy to mercury ratio by mass is approximately 1.3:1		
Dispersalloy®* (Zn-containing)	Silver	69 %
	Tin	18 %
	Copper	12 %
	Zinc	1 %
The recommended alloy to mercury ratio by mass is approximately 1:1		

* Dentsply Detrey GmbH Konstanz, Germany.

Table 2. Micro-X-ray diffraction pattern analysis approach of sound and caries-affected dentin before and after amalgam restoration.

	Amalgam treatment	Dentin area	002 plane					310 plane					*H*/*L*
			FWHM	*H*: Scherrer equation (nm) (*τ*)	Scherrer-Wilson equation (nm)	Microstrain %	R_{hkl}	FWHM	*L*: Scherrer equation (nm) (*τ*)	Scherrer-Wilson equation (nm)	Microstrain %	R_{hkl}	
Zn-Free	Before treatment*	SD	0.0129	11.51	11.23	$4.06x10^{-4}$	0.881	0.0262	5.88	5.53	$1.61x10^{-3}$	1.114	1.96
		CAD	0.0121	12.26	11.95	$3.58x10^{-4}$	0.947	0.0224	6.88	6.47	$1.18x10^{-3}$	1.111	1.78
	After treatment**	SD	0.0126	11.81	11.51	$3.86x10^{-4}$	0.937	0.0250	6.18	5.81	$1.46x10^{-3}$	1.320	1.91
		CAD	0.0132	11.23	10.95	$4.26x10^{-4}$	0.994	0.0264	5.84	5.49	$1.64x10^{-3}$	1.238	1.92
Zn-Contain.	Before treatment*	SD	0.0140	10.64	10.37	$4.75x10^{-4}$	0.489	0.0329	4.68	4.40	$2.54x10^{-3}$	0.428	2.27
		CAD	0.0132	11.27	10.99	$4.23x10^{-4}$	0.421	0.0245	6.30	5.92	$1.41x10^{-3}$	0.408	1.79
	After treatment**	SD	0.0125	11.85	11.55	$3.83x10^{-4}$	0.546	0.0225	6.85	6.44	$1.19x10^{-3}$	0.657	1.73
		CAD	0.0136	10.91	10.63	$4.52x10^{-4}$	0.476	0.0239	6.44	6.06	$1.34x10^{-3}$	0.569	1.70

*Untreated groups
** Treated groups
Abbreviations: SD: Sound dentin; CAD: Caries-affected dentin; FWHM: Full-width half-maximum